Chelators for Radioimmunotherapy: I. NMR and Ab Initio Calculation Studies on 1,4,7,10-Tetra(carboxyethyl)-1,4,7,10-tetraazacyclododecane (DO4Pr) and 1,4,7-Tris(carboxymethyl)-10-(carboxyethyl)-1,4,7,10-tetraazacyclododecane (DO3A1Pr)

David A. Keire,[†,‡] Yun Hee Jang,[§] Lin Li,[†] Siddarth Dasgupta,[§] William A. Goddard III,[§] and John E. Shively*[,†]

Materials and Process Simulation Center, Beckman Institute (139-74), California Institute of Technology, Pasadena, California 91125, The Beckman Research Institute of the City of Hope, 1450 E. Duarte Rd., Duarte, California 91010, and CURE/UCLA Digestive Diseases Research Center, UCLA School of Medicine, Los Angeles, California 90095

Received September 13, 2000

This work describes the modification of the chelating agent 1,4,7,10-tetraazacyclododecane-*N*,*N*′,*N*″,*N*‴-tetraacetic acid (DOTA) to improve the rate of metal loading for radioimmunotherapy applications. Previous ab initio calculations predicted that the compounds 1,4,7,10-tetra(carboxyethyl)-1,4,7,10-tetraazacyclododecane (DO4Pr) and 1,4,7-tris(carboxymethyl)-10-(carboxyethyl)-1,4,7,10-tetraazacyclododecane (DO3A1Pr) have a ca. 2000-fold improvement in yttrium metal loading rates compared to those of DOTA (Jang, Y. H.; Blanco, M.; Dasgupta, S.; Keire, D. A.; Shively, J. E.; Goddard, W. A., III. *J. Am. Chem. Soc.* **1999**, *121*, 6142−6151). In this study, we report the synthesis, purification, ^{1}H-NMR chemical shift assignments, pK_a values, metal loading rate measurements, and additional ab initio calculations of these two compounds. The yttrium loading rates of DO3A1Pr are approximately twice those of DOTA, at pH 4.6 and 37 °C. The NMR data indicates that the DO4Pr analogue forms a stable **type I** complex but does not form a **type II** complex. The new ab initio calculations performed on DO4Pr and DO3A1Pr indicate that the rate-determining step is the deprotonation of the first macrocycle amine proton, not the second proton as assumed in the previous calculations. The new calculations predict an improvement in the rate of metal loading that more closely matches the experimentally observed change in the rate.

Introduction

Current interest in the clinical use of chelating agents as vehicles for delivery of metals to sites in biological systems has led to the synthesis and study of a large number of new cyclic polyoxa and polyaza ligands.[1,2] For example, analogues of 1,4,7,10-tetraazacyclododecane-*N*,*N*′,*N*″,*N*‴-tetraacetic acid (DOTA) have been developed for clinical applications that involve the conjugation of the chelating agent to peptides that act on tumor receptors, antibodies targeting cancer cells for delivery of radiometals to tumor sites (radioimmunotherapy), and the use of chelated metals as contrast reagents for medical resonance imaging.[1−8] Important for the success of the radioimmunotherapy application is a chelating agent that rapidly forms a stable inert complex with a radiometal for therapy (e.g., with ^{90}Y, a β-emitter) and imaging (e.g., with ^{111}In, ^{64}Cu, or ^{67}Ga as γ- or positron-emitters).

DOTA has received attention for these biological applications because it is well know to form stable complexes with a wide variety of metal ions.[9−14] Furthermore metal−DOTA complexes have been shown to be kinetically inert under physiological conditions.[15−19] However, a limitation of these compounds for biological applications is the slow rate of formation of the fully chelated metal complex, especially for large effective ionic radii metals (e.g., Y and Gd).[19−23] For example, routine radiolabeling conditions require elevated temperatures, long reaction times

* To whom correspondence should be addressed.
[†] The Beckman Research Institute of the City of Hope.
[‡] CURE/UCLA Digestive Diseases Research Center, UCLA School of Medicine.
[§] Materials and Process Simulation Center, Beckman Institute (139-74), California Institute of Technology.

(1) Alexander, V. *Chem. Rev.* **1995**, *95*, 273−342.
(2) Caravan, P.; Ellison, J. J.; McMurry, T. J.; Lauffer, R. B. *Chem. Rev.* **1999**, *99*, 2293−2352.
(3) Liu, Y.; Wu, C. *Pure Appl. Chem.* **1991**, *63*, 427−463.
(4) Britton, K. E. *Nucl. Med. Commun.* **1997**, *18*, 992−1005.
(5) Chatal, J.-F.; Hoefnagel, C. A. *Lancet* **1999**, *354*, 931−935.
(6) Anderson, C. J.; Welch, M. J. *Chem. Rev.* **1999**, *99*, 2219−2234.
(7) Joensuu, H.; Tenhunen, M. *Acta Oncologia Suppl.* **1999**, *13*, 75−83.
(8) Volkert, W. A.; Hoffman, T. J. *Chem. Rev.* **1999**, *99*, 2269−2292.
(9) Loncin, M. F.; Desreux, J. F.; Merciny, E. *Inorg. Chem.* **1986**, *25*, 2646−2648.
(10) Cacheris, W. P.; Nickle, S. K.; Sherry, A. D. *Inorg. Chem.* **1987**, *26*, 958−960.
(11) Kumar, K.; Magerstadt, M.; Gansow, O. A. *J. Chem. Soc., Chem. Commun.* **1989**, 145−146.
(12) Broan, C. J.; Cox, J. P. L.; Craig, A. S.; Kataky, R.; Parker, D.; Harrison, A.; Randall, A. M.; Ferguson, G. *J. Chem. Soc., Perkins Trans. 2* **1991**, 87−99.
(13) Clarke, E. T.; Martell, A. E. *Inorg. Chim. Acta* **1991**, *190*, 27−36.
(14) Clarke, E. T.; Martell, A. E. *Inorg. Chim. Acta* **1991**, *190*, 37−46.
(15) Moi, M. K.; Meares, C. F.; DeNardo, S. J. *J. Am. Chem. Soc.* **1988**, *110*, 6266−6267.
(16) Meares, C. F.; Moi, M. K.; Diril, H.; Kukis, D. L.; McCall, M.; Desphandes, J.; DeNardo, S. V.; Snook, D.; Epenetos, A. A. *Br. J. Cancer* **1990**, *Suppl. 10*, 21−26.
(17) Desphande, S. V.; DeNardo, S. J.; Kukis, D. L.; Moi, M. K.; McCall, M. J.; DeNardo, G. L.; Meares, C. F. *J. Nucl. Med.* **1990**, *31*, 473−479.
(18) Li, M.; Meares, C. F. *Bioconjugate Chem.* **1993**, *4*, 275−283.
(19) Lewis, M. R.; Raubitschek, A.; Shively, J. E. *Bioconjugate Chem.* **1994**, *5*, 565−576.
(20) Desreux, J. F. *Inorg. Chem.* **1980**, *19*, 1319−1324.
(21) Kodama, M.; Koike, T.; Mahatma, A. B.; Kimura, E. *Inorg. Chem.* **1991**, *30*, 1270−1273.

10.1021/ic0010297 CCC: $20.00
Published on Web 07/19/2001

Scheme 1. The Proposed Two Step Reaction for the Formation of the Metal (M) DOTA (L) Complex

$$M^{3+} + H_2L^{2-} \quad \leftarrow \text{fast} \rightarrow \quad [M(H_2L)^+] \text{ or } [M(HL) + H^+]$$

Type I (partially coordinated)

$$\text{slow} \rightarrow \quad ML^- + 2H^+$$

Type II (fully coordinated metal)

(>1 h), and result in only 50−60% radiolabeling efficiency.[22] In recent studies, Kukis et al. have reinvestigated the conditions for radiolabeling DOTA−mAb conjugates and shown that under specific conditions of buffer and protein concentration up to 91% radiolabeling efficiency can be obtained in 30 min at 37 °C.[24] In the studies reported here, we have taken another approach, namely investigating the mechanism for metal loading and predicting structural modifications that effect faster rates of metal loading.

For yttrium and gadolinium, the formation of the fully complexed metal ion is a two-step process; initially a reversible, partially coordinated (**type I**, see Scheme 1) adduct forms followed by the slow irreversible formation of the fully coordinated metal form (**type II**).

For example, Gd-DOTA **type I** and **type II** complexes form with rate constants of ca. 50 M^{-1} s^{-1} and 10^{-3} s^{-1}, respectively. In contrast, flexible acyclic polyaza chelators form **type II** metal complexes much more rapidly than metal−DOTA **type II** complexes (e.g., the rate of formation of Y−diethylenetriamine pentaacetic acid complexes (Y-DTPA) is 1600 times faster than the rate of formation of Y−DOTA complexes[21]). Unfortunately, the added flexibility of the acyclic compounds leads to a decrease in the in vivo solution stability of these molecules compared to their cyclic analogues.[15,17,22]

One design strategy for new chelators has focused on the modification of DOTA pendant arms to improve the metal loading rates while maintaining the solution stability with the rigid tetraazamacrocycle scaffold (e.g., refs 25 and 26). These studies have been performed without a detailed understanding of the rate-determining mechanism of deprotonation of the macrocycle amines in the **type I** to **type II** reaction or the changes in DOTA chelating properties with pendant arm modification.

Various experimental results have established that the metal loading rate is pH-dependent, and two different intermediate **type I** forms have been proposed.[27−31] Critical for rapid metal loading is the facile base-catalyzed removal of the two trans macrocycle amine protons in the sterically restricted environment of the **type I** complex. Recently, we performed ab initio

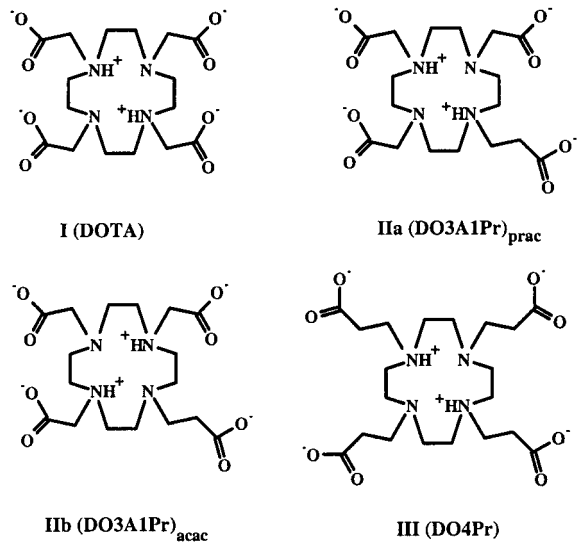

Figure 1. The structures of DOTA, DO4Pr, and DO3A1Pr.

studies on Y−DOTA complexes that indicated the most energetically favorable mechanism for deprotonation of the macrocyle amine protons involves proton transfer by the pendant arm carboxylates.[32] We predicted that addition of an additional methylene group to the DOTA acetate arms (to form propionate arms) would lead to a 2000-fold increase in the rate of yttrium metal loading compared to that of DOTA.

In this work, we synthesized and purified DO4Pr (a tetrapropionate analogue of DOTA) and DO3A1Pr (a triacetate, monopropionate analogue of DOTA) and measured their pK_a values and yttrium metal loading rates by NMR methods (Figure 1). These parameters are compared with the values previously measured for DOTA and butylamine−DOTA under identical conditions.[23] The NMR results reveal a 2-fold increase in the rate of metal loading in DO3A1Pr relative to that of DOTA and the formation of a stable **type I** complex for DO4Pr. Additional ab initio calculations performed on the DOTA analogues indicate that the deprotonation of the first of the macrocycle amine protons is rate limiting; this is in contrast to the previous assumption that the deprotonation of the second macrocycle amine proton was rate limiting.

Experimental Section

Synthesis and Purification of DO4Pr and DO3A1Pr. DO4Pr. Cyclen (50 mg, 0.29 mmol, Macrocyclic Inc.) in 2 mL of low metal water (pH 12) was added dropwise to 3-bromopropionic acid (0.44 g, 2.9 mmol, Aldrich) in 2 mL of low metal water (pH 2) with strirring and constant adjustment of the pH to 9−10 with 6 M KOH. The reaction was continued for 24 h at RT at pH 9−10. The reaction mixture was acidified to pH 2.5 with 1 M HCl and loaded onto a Dowex AG50W−X8 column (6 mL, H^+ form) that was washed with 200 mL of water and eluted with 10 mL each of 0.5, 1.0, 2.0, and 4.0 M NH_4OH. Fractions (1 mL) were dried (Savant) and analyzed by ESI−MS (Finnigan Iontrap LCQ). Fractions 8−29, which were found to contain the tetra-substituted derivative, were pooled, the pH adjusted to 11, and applied to a Dowex AG1-X4 column (12 mL, formate form). The column was washed with 200 mL of water and eluted with 10 mL each of 0.05, 0.1, 0.2, and 0.5 M formic acid. Fractions (1 mL) were dried twice (Savant) and analyzed by ESI−MS (expected $M + H^+ = 461.26$; observed, 461.23). The combined yield was 16.2 mg of white powder.

DO3A1Pr. DO3A tri-*tert*-butyl ester (100 mg, 0.19 mmol, Macrocyclics, Inc.) was dissolved in 3.0 mL of 95% TFA and stirred at room

(22) Stimmel, J. B.; Stockstill, M. E.; Kull, F. C. J. *Bioconjugate Chem.* **1995**, *6*, 219−225.
(23) Keire, D. A.; Kobayashi, M. *Bioconjugate Chem.* **1999**, *10*, 454−463.
(24) Kukis, D. L.; DeNardo, S. J.; DeNardo, G. L.; O'Donnell, R. T.; Meares, C. F. *J. Nucl. Med.* **1998**, *39*, 2105−2110.
(25) Takenouchi, K.; Watanabe, K.; Kato, Y.; Koike, T.; Kimura, E. *J. Org. Chem.* **1993**, *58*, 1955−1958.
(26) Takenouchi, K.; Tabe, M.; Watanabe, K.; Hazato, A.; Kato, Y.; Shionoya, M.; Koike, T.; Kimura, E. *J. Org. Chem.* **1993**, *58*, 6895−6899.
(27) Kasprzyk, S. P.; Wilkins, R. G. *Inorg. Chem.* **1982**, *21*, 3349−3352.
(28) Brucher, E.; Laurenczy, G.; Makra, Z. S. *Inorg. Chim. Acta* **1987**, *139*, 141−142.
(29) Wang, X.; Jin, T.; Comblin, V.; Lopez-Mut, A.; Merciny, E.; Desreux, J. F. *Inorg. Chem.* **1992**, *31*, 1095−1099.
(30) Kumar, K.; Tweedle, M. F. *Inorg. Chem.* **1993**, *32*, 41934199-.
(31) Wu, S. L.; Horrocks, W. D. J. *Inorg. Chem.* **1995**, *34*, 3724−3732.
(32) Jang, Y. H.; Blanco, M.; Dasgupta, S.; Keire, D. A.; Shively, J. E.; Goddard, W. A. I. *J. Am. Chem. Soc.* **1999**, *121*, 6142−6151.

temperature for 24 h. The product was dried (Savant) and found to contain only DO3A by ESI−MS ($M + H^+ = 347.0$). The product was dissolved in 3 mL water, the pH adjusted to 9 with 6 M KOH, and reacted with 3-bromopropionic acid (116 mg, 0.38 mmol) in 1 mL of water for 24 h with stirring at RT. A second aliquot of 3-bromopropionic acid was added, and the reaction was continued at pH 9 for an additional 2 days. The pH was adjusted to 2, and the product purified as described above. The product had the expected mass by ESI−MS (expected $M + H^+ = 419.21$; observed, 419.30). The final yield was 35 mg (57%).

Exact Mass Determination. The molecular formulas of DO3A1Pr and DO4Pr were confirmed by exact mass analysis on a Micromass ZAB 7070 magnetic sector mass spectrometer using LSIMS (CsI). The observed (versus expected) monomasses were 441.196134 (441.197100) for the sodium salt of DO3A1Pr (formula C17 H30 N4 O8 Na), and 483.243084 (483.245500) for the sodium salt of D04Pr (formula C20 H36 N4 O8 Na).

Calculation Details. All of the calculations were performed with Jaguar v3.5[33] at the B3LYP//HF level. This method calculates the single-point energy at the B3LYP level,[34,35] with the geometry optimized at the Hartree−Fock level using the LACVP* basis set. This basis set is constituted of the 6-31G* basis (double ζ plus polarization) for C, O, N, and H (no polarization) and only the outermost electrons for the metals (e.g., 4s4p5s for Y). The core electrons for the metal (1s2s2p3s3p3d) are replaced by the effective core potentials (ECP) of Hay and Wadt.[36] The number of basis functions are 462 for $Y(DOTA)^-$, 464 for YH(DOTA), and 466 for $YH_2(DOTA)^+$. The calculated stationary points were characterized by the vibrational frequencies from the Hessian, where all frequencies are real for a true minimum, and one and only one frequency is imaginary for a saddle point (transition state).

The solvent effect of water were treated in the continuum-solvation approach[37−39] by solving the Poisson−Boltzmann (PB) equation numerically.[40] In this approach, the solute is described as a low-dielectric ($\epsilon = 1$) cavity immersed in a high-dielectric continuum of solvent ($\epsilon = 80$ for water). The solute/solvent boundary is described by a contact surface−the surface of closest approach as a sphere of radius 1.4 Å (probe radius for water) is rolled over the van der Waals (vdW) envelope of the solute. The charge distribution of the solute is represented by a set of atom-centered point charges, which are determined by fitting the electrostatic potential calculated from the ab initio wave function. A gas-phase calculation is carried out first to obtain these electrostatic-potential (ESP) fitted charges. Based on these, the reaction field of the solvent is obtained as a set of polarization charges located on the solute/solvent boundary surface by solving the PB equation. A new Hamiltonian for solute−solvent interaction is calculated in the presence of this reaction field, leading to a new wavefunction and a new set of atom-centered ESP charges. This process is repeated self-consistently until convergence (0.1 kcal/mol in solvation energy) is reached. This is the electrostatic or "polar" contribution to the solvation energy. A "nonpolar" contribution, due to the creation of a solute cavity in the solvent, is accounted for by a term proportional to the solvent-accessible surface area of the solute.[37,38] The atomic radii used to build the vdW envelope of the solute are taken from van der Waals radii used in the DREIDING force field (1.9 Å for C, 1.6 Å for O and N, and 1.15 Å for H)[37,41] and are slightly modified to reproduce the experimental solvation energy in water. The radius for Y is 1.807 Å, which gives the solvation energy of −826.1 kcal/mol, while the experimental free energy of solvation is -825[42] ~ -826.2 kcal/mol.[43]

Table 1. Energetics (in kcal/mol) Involved in Two Pathways of Deprotonation of $YH_2(DOTA)$

$YH_2(DOTA)$	H_2Y to H_1Y	H_1Y to H_0Y	activation barrier
N−to−O proton transfer	22.4 (new)	12.2	
4-coord to 3-coord	16.6	21.6	
barrier of each conversion step	16.6	12.2	16.6

NMR Measurements. NMR experiments were performed on a Varian Unity Plus 500 MHz spectrometer (Varian Instruments, Palo Alto, CA), with the probe air temperature regulated at 37 °C. NMR studies on DO3A1Pr and DO4Pr in solution were performed at 1−2 mM concentrations in 90% H_2O/10% D_2O solutions, with the pH adjusted by addition of HCl or NaOH. All pH measurements were performed with an Orion model 601 pH meter equipped with a combination electrode for 5 mm NMR tubes (Ingold Electrodes, Wilmington, MA). Standard aqueous buffers were used for electrode calibration at pH 4 and 7. All chemical shifts were referenced to the methyl proton signal of sodium-2,2-dimethyl-2-silapentane-5-sulfonate (DSS, at 0 ppm), which was either external or added to the samples.

The assignment of the pH-dependent chemical shifts for DO3A1Pr protons was aided by the observed magnitude of the chemical shift changes during the titration of proximate acidic groups. Those carbon-bonded protons closest to the deprotonation site generally have the largest increase in shielding and, concomitantly, the largest chemical shift changes to lower ppm values. The assignments were confirmed by total correlation spectroscopy (TOCSY[44]) spectra connectivities at selected pHs. Typically, the TOCSYs were performed with 2K points collected in t_2 (32−48 transients per increment), and 256 complex points in t_1.[45] The transmitter channel was used for excitation and observation of the 6000 Hz proton frequency range as well as presaturation of the H_2O signal. Data were processed with zero filling to 2K points in F1 and shifted sine-bell apodization functions in both F1 and F2.

The DO3A1Pr **type I** to **type II** rate constant (k*) was determined, as a function of pH, by measuring the intensity of the **type I** and **type II** forms, as a function of time, after the addition of excess yttrium. Typically, 750 μL of a 1 mM DO4Pr or DO3A1Pr solution was made in 90% H_2O/10% D_2O, the pH adjusted to the desired value with 1 M KOH and 1 N HCl, and a 1D spectrum was acquired. Subsequently, 62 μL of a 65 mM yttrium chloride stock solution was added to the NMR tube (ca. 5 mM), and a series of spectra were acquired as a function of time over 10−14 h. The peak areas of the signals from the acetate methylene group protons in the **type I** and **type II** forms were measured from each time-course data set and plotted.

Acid-Dissociation Constants. Acid dissociation constants were determined by fitting the NMR chemical shift titration data to monoprotic and diprotic acid models by nonlinear least-squares methods previously described.[23,46,47] The criteria used to select a model were the number of observed inflection points and comparison of the χ^2 values obtained from fitting the data to monoprotic and diprotic models. The DO3A1Pr k* for yttrium was determined by the method of initial rates. The fitting of the acid dissociation and rate constants was performed with Mathematica 3.0 (Wolfram Research, Champaign, IL).

Results

Calculations on DOTA Analogues, $YH_2(DOTA)$ versus YH(DOTA): What is the Rate-Determining Step? The energetics of each deprotonation process from $YH_2(DOTA)$ to

(33) *Jaguar*, Version 3.5; Schrodinger Inc.: Portland, OR, 1998.
(34) Becke, A. D. *J. Chem. Phys.* **1993**, *98*, 5648−5652.
(35) Lee, C. T.; Yang, Y. T.; Parr, R. G. *Phys. Rev. B*: *Condens. Matter Mater. Phys.* **1988**, *37*, 785−789.
(36) Hay, P. J.; Wadt, W. R. *J. Chem. Phys.* **1985**, *82*, 270.
(37) Tannor, D. J.; Marten, B.; Murphy, R.; Friesner, R. A.; Sitkoff, D.; Nicholls, A.; Ringnalda, M. N.; Goddard, W. A., III; Honig, B. A. *J. Am. Chem. Soc.* **1994**, *116*, 11875.
(38) Marten, B.; Kim, K.; Cortis, C.; Friesner, R. A.; Murphy, R. B.; Ringnalda, M. N.; Sitkoff, D.; Honig, B. *J. Phys. Chem.* **1996**, *100*, 11775.
(39) Honig, B.; Nicholls, A. *Science* **1995**, *268*, 1144.
(40) Nicholls, A.; Honig, B. *J. Comput. Chem.* **1991**, *12*, 435.
(41) Mayo, S. L.; Olafson, B. D.; Goddard, W. A., III *J. Phys. Chem.* **1990**, *94*, 8897.
(42) Marcus, Y. *J. Chem. Soc., Faraday Trans.* **1991**, *87*, 2995.
(43) Marcus, Y. *Ion Solvation*; John Wiley and Sons: New York, 1985.
(44) Braunschweiler, L.; Ernst, R. R. *J. Magn. Reson.* **1983**, *53*, 521−528.
(45) States, D. J.; Haberkorn, R. A.; Ruben, D. J. *J. Magn. Reson.* **1982**, *48*, 286.
(46) Jardetzky, O.; Roberts, G. C. K. *NMR in Molecular Biology*; Academic Press: New York, 1981.
(47) Keire, D. A.; Robert, J. M.; Rabenstein, D. L. *J. Org. Chem.* **1992**, *57*, 4427−4431.

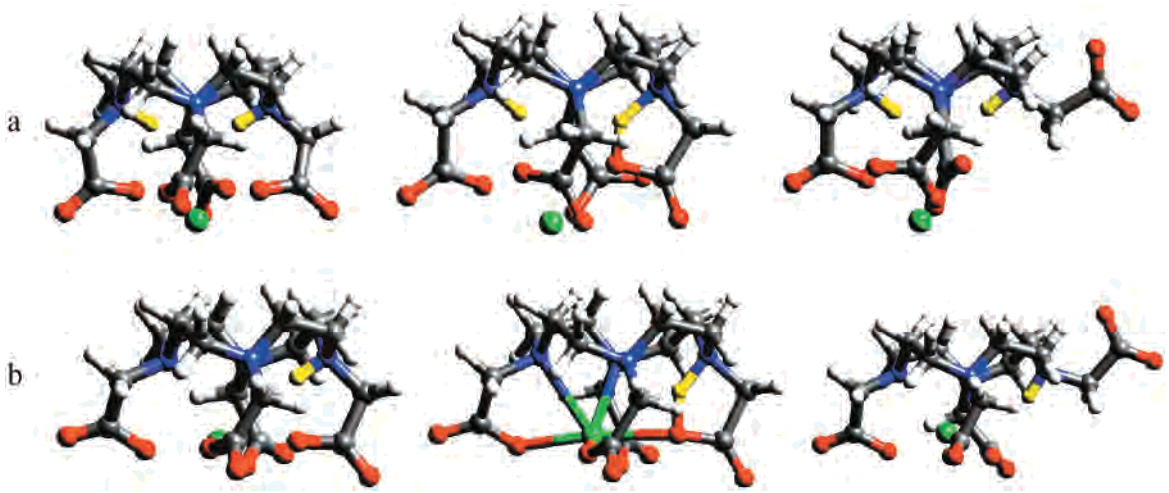

Figure 2. Two pathways to deprotonation (N−to−O proton transfer and cage-opening) of (a) $YH_2(DOTA)^+$ and (b) YH(DOTA). Color scheme; amine protons (yellow), nitrogen (blue), carboxylate oxygen (red), carbon (grey), carbon-bound protons (white), and yttrium (green).

Table 2. Energetics Involved in Two Pathways of Deprotonation of (a) $YH_2(DOTA)$ and (b) $YH_2(DO3A1Pr)$. The Rate Is Approximately Calculated Based on Energy, Not on Free Energy

	H_2Y to H_1Y	H_1Y to H_0Y	activation barrier	rate
(a) $YH_2(DOTA)$				
N−to−O proton transfer	22.4	12.2		
4-coord to 3-coord	16.6	21.6		
barrier of each conversion step	16.6	12.2	16.6	1
(b) $YH_2(DO3A1Pr)_{prac}$[a] (85%)				
N−to−O proton transfer (on Pr)	15.0	4.5		
4-coord to 3-coord (with Ac)	13.7	>21.6		
barrier of each conversion step	13.7	4.5	13.7	∼134
(b) $YH_2(DO3A1Pr)_{acac}$[a] (15%)				
N−to−O proton transfer (on Ac)	∼22.4	∼12.2		
4-coord to 3-coord (with Ac)	15.7	>21.6		
barrier of each conversion step	15.7	∼12.2	15.7	∼5

[a] $YH_2(DO3A1Pr)_{prac}$ has a ring proton on N−Pr (a ring nitrogen attached to propionate arm) and the other on the opposite N−Ac (a ring nitrogen attached to acetate arm), and the $YH_2(DO3A1Pr)_{acac}$ has a ring proton on N−Ac and the other on the opposite N−Ac.

Y(DOTA) are summarized in Table 1. The energy barrier of the N−to−O proton transfer for $YH_2(DOTA)$ is 22.4 kcal/mol, which is much higher than the 12.2 kcal/mol calculated for the YH(DOTA) deprotonation. The higher barrier for $YH_2(DOTA)$ than for YH(DOTA) can be explained as follows. The hydrogen is located farther from the carboxylate oxygen in $YH_2(DOTA)$ than in YH(DOTA). The H···O distance in the 4-coordinate $YH_2(DOTA)$ is 2.2 Å, while that in the 4-coordinate YH(DOTA) is 1.8 Å (Figure 2 and Supporting Information Table 1). The N−H···O hydrogen bonding is less favorable in $YH_2(DOTA)$ than in YH(DOTA). Thus, for the proton-transfer reaction to occur in $YH_2(DOTA)$, a carboxylate arm should move toward the inside of the cage. The conformation changes a great deal from reactant to TS in the proton-transfer reaction of YH_2-(DOTA) (RMS deviation ∼ 0.47 Å), while the conformation hardly changes in the case of YH(DOTA) (RMS deviation ∼ 0.12 Å). With this movement of the highly soluble carboxylate arm, the transition state becomes much less favorable in solvation than the reactant in the case of $YH_2(DOTA)$ (the decrease of solvation energy from reactant to TS is 21.2 kcal/mol, compared with 10.1 kcal/mol in the case of YH(DOTA); Supporting Information Table 2). Thus, the conversion from $YH_2(DOTA)$ to YH(DOTA) occurs through the conformation change from 4-coordinate to 3-coordinate (the cage opening), which needs a lower energy input of 16.6 kcal/mol.

The conversion from YH(DOTA) to Y(DOTA) requires the energy cost of 12.2 kcal/mol, and the rate-determining step is the conversion from $YH_2(DOTA)$ to YH(DOTA) rather than the conversion from YH(DOTA) to Y(DOTA), as we assumed in our previous work. This result is consistent with the finding of Mäcke et al., that they could crystallize $MH_2(DOTA)$ but not MH(DOTA) [H. Mäcke et al., private communication]. Preliminary calculations adding a zero-point energy and ΔG (0 to 298 K) to the above energy data (Supporting Information Table 2) to obtain the free energy information and suggest that this correction does not change the conclusions derived above.

DO3A1Pr. The situation is more complicated for DO3A1Pr since there are two isomers of $YH_2(DO3A1Pr)$, YH_2-$(DO3A1Pr)_{prac}$ (**IIa**) and $YH_2(DO3A1Pr)_{acac}$ (**IIb**). The YH_2-$(DO3A1Pr)_{prac}$ has a ring proton on N−Pr (a ring nitrogen attached to a propionate arm) and the other on the opposite N−Ac (a ring nitrogen attached to an acetate arm, denoted by the subscript prac), and the $YH_2(DO3A1Pr)_{acac}$ has a ring proton on N−Ac and the other on the opposite N−Ac (denoted by the subscript acac). The energy difference between these two isomers is only 1.0 kcal/mol, which is even smaller than the uncertainty in the current Gibbs free energy correction calculated from the approximate Hessian matrix. Based on the energy difference, $YH_2(DO3A1Pr)$ is present as 85% of YH_2-$(DO3A1Pr)_{prac}$ and 15% of $YH_2(DO3A1Pr)_{acac}$. These two isomers have different energy barriers of deprotonation, as given in Table 2. Similar to the DOTA case, the calculations show that the deprotonation of the first macrocycle amine nitrogen of the major form of DO3A1Pr requires a greater movement of the solvated pendant groups than the singly protonated form (Table 3). In this case, the cage-opening mechanism is the lower energy path to deprotonation, while the proton-transfer mechanism is the more favored path for the second proton (Support-

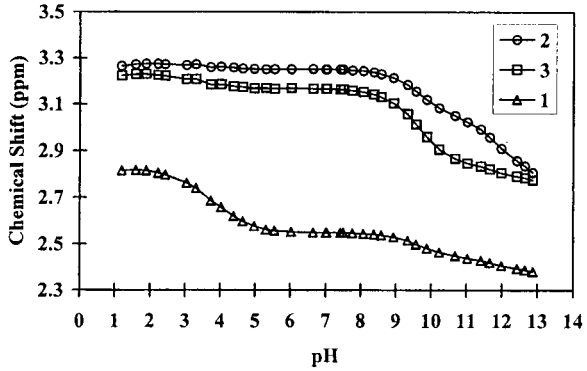

Figure 3. Plots of the chemical shifts of the side chain (carboxylate (1), and nitrogen (2) adjacent) and macrocycle ring (3) protons of DO4Pr as a function of pH.

Table 3. Geometry Change from Reactant to TS in the Proton Transfer Reaction of YH_2(DO3A1Pr)

	(a) $YH_2(DO3A1Pr)_{prac}$		(b) $YH(DO3A1Pr)_{pr}$	
	reactant	TS	reactant	TS
r(O−Y) (Å)	2.18	2.15	2.19	2.18
	2.19	2.32, 2.55	2.19	2.18
	2.25	2.19	2.22	2.21
	2.25	2.37	2.27	2.37
r(H−Y) (Å)	3.76, 3.14	3.32, 3.08	2.99	2.87
r(N−Y) (Å)	3.95	3.95	2.72	2.66
	4.14	4.14	2.88	2.75
	4.31	4.31	3.31	3.16
	4.74	4.74	3.98	3.92
r(N−H) (Å)	1.03, 1.01	1.43, 1.01	1.03	1.24
r(H···O) (Å)	1.68, 2.34	1.06, 2.39	1.61	1.18

ing Information, Figure 1). The weighted average rate of DO3A1Pr is 114-fold higher than that of DOTA. However, this estimate of the rate is very crude because of the lack of more accurate estimation of the free energy correction.

NMR pH Titrations. DO4Pr and DO3A1Pr have multiple sites with Brönsted acid/base properties in aqueous solution. For DO4Pr, these are the four carboxylic acid groups and two protonated macrocycle nitrogen protons. Over the range pH 0−13 these groups undergo protonation/deprotonation reactions, and the chemical shifts of the carbon-bonded protons near sites of protonation or deprotonation are expected to change due to through-bond electrostatic effects.[46] Thus, acid dissociation constants were determined for these groups from the dependence of the chemical shifts of the carbon-bonded protons on pH.

The NMR spectrum of DO4Pr in aqueous solution consists of three signals, two for the pendant ethylene group protons and the third for the macrocycle ethylene protons. The NMR pH titration data of the DO4Pr proton signals are shown in Figure 3. Signals for the protons on the macrocycle nitrogens are not observable because of exchange broadening.[48] Instead, the presence of nitrogen-bound protons in the macrocycle is inferred by the pH dependence of the chemical shifts of other nearby carbon-bonded proton signals at basic pHs.

Macroscopic acid dissociation constants were determined for the various groups by fitting the NMR pH titration data to monoprotic and diprotic models, as previously described.[23] The chemical shift values of the fully deprotonated and fully protonated forms of DO4Pr titratable groups (and the intermediate value in the diprotic model) are also obtained from the fits of the NMR pH titration data. The values obtained for the DO4Pr pK_as and the titration shifts for the propionic acid and

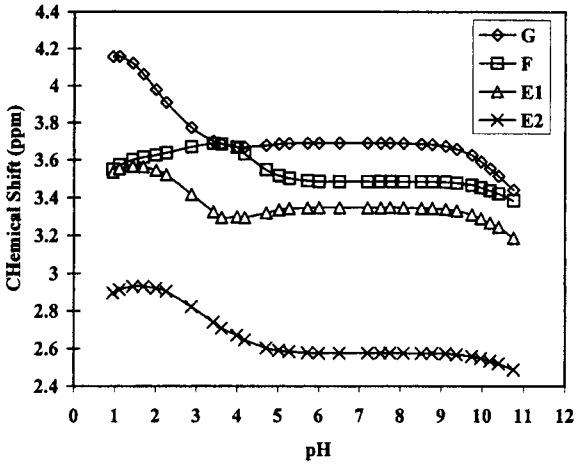

Figure 4. A plot of the chemical shifts of the DO3A1Pr G, F, E1, and E2 methylene proton signals as a function of pH.

macrocycle ethylene protons are listed in the Supporting Information Table 3.

The measured pK_a values are assigned to protonation of two trans amine nitrogens (designated G amines, microscopic pK_as of 9.62 and 11.92), the two carboxyl groups near the nonprotonated amines (designated F carboxylates, macroscopic pK_a 4.44), and the titration of the remaining two carboxylic acid groups nearest the protonated amines (designated G carboxylates, macroscopic pK_a 3.58). The individual pK_as of the F and G carboxylate's protons were calculated using the relationship between macroscopic and microscopic protonation constants.[49] The calculated DO4Pr pK_a values of the G carboxlates, the F carboxylates, and the G amine protons are 3.22, 3.74, 4.28, 4.80, 9.62, and 11.92, respectively (Supporting Information Table 3).

NMR pH Titration of DO3A1Pr. The conjugation of bromopropionic acid with trisubstituted-DOTA active ester to form DO3A1Pr greatly increases the number of NMR signals present, whereas only three signals were observed in DO4Pr spectra (compare Figures 5 and 6). For example, in the conjugate, separate NMR peaks are observed for the acetate and ethylene signals directly adjacent (labeled E1, E2, and E amine) and opposite (G and G amine) to the site of the modification because the molecule is no longer symmetric; in symmetrical DO4Pr these signals overlap. The separate signals allow for the measurement of the microscopic protonation constants of the four carboxylic acid groups and the two macrocyle amines via fits of the pH-dependent chemical shifts of proximal carbon-bonded protons.

The ^{1}H NMR resonances of DO3A1Pr were individually assigned by comparison with DO4Pr chemical shifts, their pattern of chemical shift changes with pH, relative intensities, and TOCSY spectra that indicated connectivities between adjacent ethylene protons (selected spectra as a function of pH are shown in the Supporting Information, Figure 2). For example, the methylene protons of the DO3A1Pr acetate arm opposite the propionic acid substitution (Figure 4, G protons) exhibit the largest chemical shift change with titration of its carboxylic acid. Similarly, the methylene groups on the carboxylic acids not attached to a protonated nitrogen (Figure 4, F protons) show a smaller perturbation with titration of the two macrocycle nitrogen protons.

The acetate methylene proton signals (F and G) shift and change shape as a function of the protonation state of DO3A1Pr.

(48) Brucher, E.; Cortes, S.; Chavez, F.; Sherry, A. D. *Inorg. Chem.* **1991**, *30*, 2092−2097.

(49) Edsall, J. T.; Wyman, J. *Biophysical Chemistry*; Academic Press: New York, 1958.

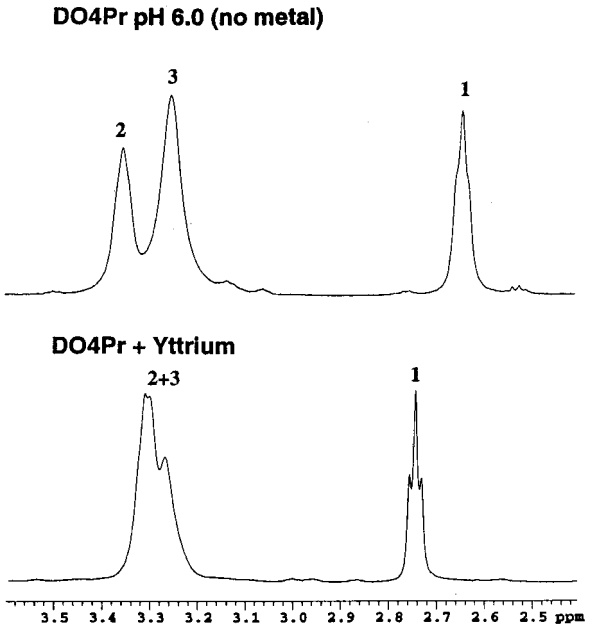

Figure 5. The 2.4−3.6 ppm region of the 500 MHz ^{1}H NMR spectra of (top) a 1 mM solution of DO4Pr at pH 6, (bottom) the same solution as in A six minutes after adding 5 mM Y. All solutions were 90% H_2O/10% D_2O, and the probe air temperature was regulated at 37 °C.

For example, the F and G acetate methylene signals at a solution pH of 2 have separate signals. Upon deprotonation of the G carboxylate, these signals move together and overlap. The F and G signals become nonequivalent again upon deprotonation of the F carboxylic acid groups. The DO3A1Pr acetate methylene and propionate methylene proton titration shift data were fit to monoprotic or diprotic models to determine the pK_as of the various functional groups and titration shifts (for titration shifts see Supporting Information Table 4). The pK_a values of the G and E carboxlates, the F carboxylates, the E amine, and the G amine protons are 2.20, 2.88, 4.00, 4.68, 9.87, and 11.07, respectively (Supporting Information Table 4).

In addition to the acid dissociation constants, the NMR titration shift data shows evidence for pH-dependent conformational changes. The increased shielding (shift to lower chemical shift value) of the methylene signals is expected due to the increased electron density in the adjacent deprotonated carboxylic acid group. Typically, in the absence of structural alterations, the closer the carbon-bonded proton to the site of the deprotonation, the greater the magnitude of the chemical shift change. By contrast, deprotonation events that lead to deshielding (movement to higher chemical shift values) for carbon-bonded protons more than 3 to 5 bonds distant from the site of deprotonation indicate the presence of conformation-dependent through-space interactions.

In particular, the formation of hydrogen bonds between amines and carboxylate groups can be identified from observation of deshielding chemical shift changes as a function of pH.[50] The chemical shifts change because the N−H bond becomes strongly polarized when the amine or amide proton forms a hydrogen bond; the proton is deshielded and its resonance shifted to higher chemical shift values. Furthermore, the deshielding tends to occur upon titration of carboxylic acid groups because a deprotonated carboxylate forms a stronger hydrogen bond than the protonated form.

Deshielding chemical shift changes attributed to the formation of hydrogen bonds and/or conformational changes are evident

(50) Bundi, A.; Wuthrich, K. *Biopolymers* **1979**, *18*, 299−311.

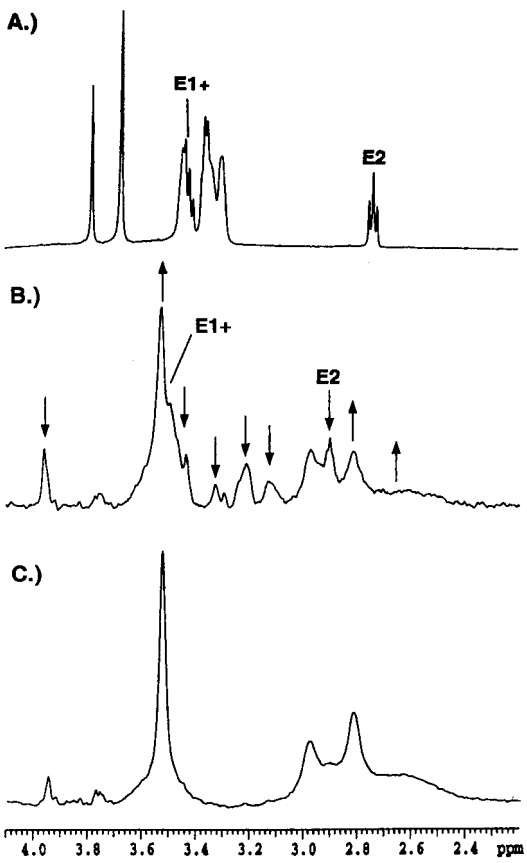

Figure 6. The 0.7−4.4 ppm region of the 500 MHz ^{1}H NMR spectra of A) a 1 mM solution of DO3A1Pr at pH 7.1, B) a solution of 1 mM DO3A1Pr at pH 4.6 six minutes after adding 5 mM Y, and C) the same solution as in B acquired ca. 24 h after adding metal. All solutions were 90% H_2O/10% D_2O, and the probe air temperature was regulated at 37 °C. Spectra B and C were acquired and displayed with the same parameters. The methylene proton signals of the propionate pendant arm, E1 and E2, are labeled in spectra A and B. The up and down arrows of spectrum B indicate signals from the **type II** and **type I** Y−DO3A1Pr complex, respectively, that increase and decrease as a function of time.

in the NMR pH titration data of DO3A1Pr (Supporting Information Table 4). For example, the F acetate methylene signal upon titration of the G carboxylic acid group shifts to a higher (deshielded) chemical shift value. In addition, with the deprotonation of the F carboxylates, the E1 methylene is deshielded. Translation of these deshielding chemical shift changes into the structures of the various protonation sates of DO3A1Pr is difficult because the observed chemical shift changes are concentration weighted averages of the different isomers present at a particular pH. Similar deshielding titration shifts have been observed in another DOTA analog.[23]

Yttrium−DO4Pr Interaction. Previous work in our laboratory has shown that yttrium metal loading into DOTA over time can be monitored by proton NMR spectroscopy.[23] For DOTA, the rate of the formation of **type I** complexes is such that by the time the first NMR spectrum is collected after adding excess metal, the chelator is a mixture of the **type I** and **type II** forms. In the presence of the metal, the NMR signals broaden and shift, and, over a period of hours, several of the broad signals disappear. The transition from the **type I** to **type II** complex is reflected in the NMR spectra of the chelator by a number of new signals appearing upon coordination of the metal by the macrocycle nitrogens.

In contrast, the NMR data suggests that DO4Pr binds yttrium in the **type I** form but does not react further to form the **type**

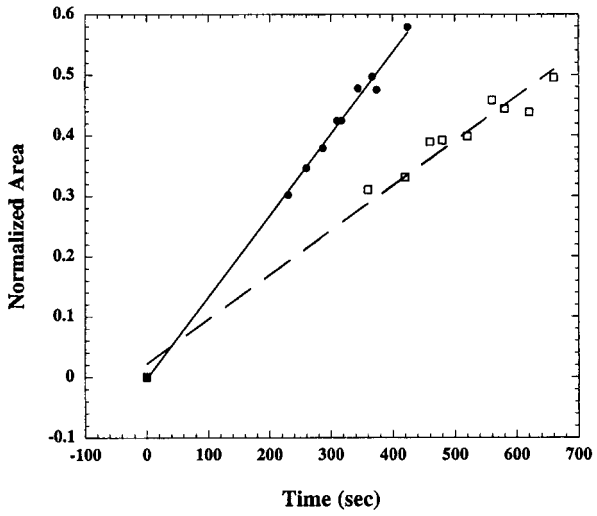

Figure 7. A comparison of the initial rates of DOTA (empty squares) and DO3A1Pr (filled circles) at pH 4.6 and 37 °C. These composite data sets were created by interleaving normalized peak area values at different time points from three different experiments for each chelator. The lines through the data sets are the best-fit lines: slopes of 1.34×10^{-3} and 0.73×10^{-3} and correlation coefficients of 0.996 and 0.987 were calculated for the DO3A1Pr and DOTA composite data sets, respectively.

II complex. The NMR spectrum of DO4Pr without metal present consists of three signals (shown in Figure 5 top, at pH 6.0 and 37 °C). Six minutes after the addition of a 5-fold molar excess of yttrium these three signals shift and narrow (shown in Figure 5 bottom), and no further changes are observed in the NMR spectrum over a period of 24 h. These changes are consistent with the formation of a four coordinate **type I** complex between the metal and the carboxylic acids of the DO4Pr. The lack of further change in the spectrum suggests that coordination of the macrocycle amines does not occur.

The chemical shift changes that occur upon addition of yttrium to a solution of DO4Pr also indicate **type I** complex formation. The chemical shift differences ($\delta_{(\text{no metal})} - \delta_{(\text{metal present})}$) of the three DO4Pr signals are −34, −15, and 8 Hz, respectively, for signals 1 (carboxylate adjacent methylene), 2 (amine adjacent side chain methylene), and 3 (macrocycle ring protons) at pH 4.6 and 37 °C. Consistent with **type I** complex formation, the largest chemical shift change in the presence of metal is observed for the methylene groups directly bonded to the carboxylic acids of DO4Pr.

Of note, further evidence for the lack of **type II** metal binding by DO4Pr is observed in the NMR pH titration data. The fully deprotonated forms of DO3A1Pr, DOTA, and butylamide−DOTA bind potassium (or other salts), which results in severe broadening of the existing signals (via quadrupolar relaxation) and the appearance of several new broad signals in the NMR spectra at basic pHs.[23] For DO4Pr, three sharp signals were observed to pH 13. Thus, for DO4Pr, we propose that the quadrupolar broadening does not occur because potassium ions are not stably incorporated into the macrocycle ring in a **type II** complex.

Yttrium Metal Loading Rates in DO3A1Pr. The rate of the formation of the **type II** complex of Y−DO3A1Pr from the **type I** complex was determined by NMR methods for comparison to the Y−BD and Y−DOTA values (Table 4). NMR spectra were collected, as a function of time, after the addition of a 5-fold excess of Y to DO3A1Pr in aqueous solution. Immediately after mixing, signals from both the **type I** and **type II** forms are present. To determine the initial rates, the decrease in the intensity of the **type I** resonances 3.23 ppm was plotted as a function of time after adding metal (Figure 6B to 6C).

Table 4. Rate Constants for Yttrium Metal Loading (**Type I** to **Type II**) in DOTA and Other Analogs at pH 4.6 and 37 °C

pH	n	k_1 (s^{-1})
DOTA[a]	8	$0.84\ (\pm 0.07) \times 10^{-3}$
BD[a]	4	$0.45\ (\pm 0.02) \times 10^{-3}$
DO3A1Pr	4	$1.61\ (\pm 0.14) \times 10^{-3}$
DO4Pr	4	−[b]

[a] Keire and Kobayashi, 1999. [b] No **type I** to **type II** transition observed.

To illustrate the ca. 2-fold difference in yttrium metal loading in DO3A1Pr and DOTA, a plot of the normalized signal area for the initial time points from replicate experiments for each chelator is presented in Figure 7. These composite data sets were created by interleaving time points from three different experiments for each chelator. The rate constants for the DO3A1Pr and DOTA composite data sets are 1.34×10^{-3} and 0.74×10^{-3} s^{-1}, respectively, and differ by a factor of 1.8. These values are slightly less than those that were measured separately from a greater number of data sets and the mean determined (Table 4). The line through the points in the best fit of the data, and the deviation of the points of the line denotes the precision of the measurement; the correlation coefficient values (r^2) are 0.996 and 0.987, respectively, for DO3A1Pr and DOTA.

Discussion

This work demonstrates the utility of chelate synthesis, NMR studies, and ab initio calculations in the design of chelating agents for radioimmunotherapy applications. The NMR experimental results suggested modifications in the ab initio models to improve the predictive accuracy of the calculations. This work describes the first iteration of a process for developing an accurate model for the mechanism and energetics of metal loading in tetraazamacrocycles.

New Calculations. DO3A1Pr (**II**) is a derivative of DOTA (**I**) that has one propionate arm in place of an acetate arm. In our previous work, we proposed that this new derivative, DO3A1Pr, would have its rate constant 2000-fold higher than that of DOTA.[32] However, after synthesizing this new derivative and measuring its rate of complexation with Y, it turned out that its increase of rate constant is only 2-fold (this work). Here we re-examined the energetics involved in each step of Y complexation of each derivative to explain this discrepancy. A four-propionate derivative DO4Pr (III) was also synthesized, and it was found that this does not form a **type II** complex with Y at all. We also investigated this case.

The assumption in the previous work was that the conversion of $\mathbf{H_1Y}$ into $\mathbf{H_0Y}$ is the rate-determining step in the following complexation scheme.

$$\underset{H_2Y}{M^{3+} + H_2L^{2-}} \overset{fast}{\rightleftharpoons} \underset{H_1Y}{[M(H^*{}_2L)^+]} \overset{fast}{\longrightarrow} \underset{H_0Y}{[M(H^*L) + H^+]} \overset{slow}{\longrightarrow} ML^- + 2H^+$$

In this work, we checked this assumption by calculating the energetics involved in the $\mathbf{H_2Y}$−to−$\mathbf{H_1Y}$ conversion. We still assume that there are two ways of $\mathbf{H_2Y}$−to−$\mathbf{H_1Y}$ conversion; that is, deprotonation from ring nitrogen, as we assumed in the previous work on $\mathbf{H_1Y}$−to−$\mathbf{H_0Y}$ (see Supporting Information,

Figure 3): one is the internal proton transfer from ring nitrogen to carboxylate oxygen leading to spontaneous exposure of proton to outside base (see Supporting Information, Figure 3a), and the other is the conformation change from cage-like 4-coordinate one to more open 3-coordinate one, leading to the exposure of ring proton to outside base in solvent (see Supporting Information, Figure 3b). We assume that (1) the latter process is a simple endothermic one, with energy increase from reactant to product without any transition state between them, and (2) the proton abstraction by outside base after the cage opening is very fast with much less energy barrier.

For DO3A1Pr, the ab initio calculations show that the new propionate arm facilitates the N−to−O proton transfer significantly by forming a six-membered ring-type transition state, and the energy barrier of first deprotonation via the proton transfer is now 15.0 kcal/mol (7.4 kcal/mol lower than 22.4 cal/mol of DOTA). The propionate arm hinders the cage-opening conformation change for same reason, because this conformation change needs to break a six-membered ring-type hydrogen bond between the ring NH and the propionate arm. Instead, the cage opening would proceed by its acetate arm, and we can expect that the energetics involved in this pathway would not change much from that of DOTA. This turned out to be true: the energy cost of cage opening of DO3A1Pr is 13.7 kcal/mol which is ∼3 kcal/mol lower than 16.6 kcal/mol of DOTA. In conclusion, the first deprotonation of DO3A1Pr can proceed via the cage opening of its acetate arm and/or the N−to−O proton transfer to its propionate arm, with the energy barrier of 14∼15 kcal/mol. This is much higher than the energy barrier for the second deprotonation of DO3A1Pr (4.5 kcal/mol). Again, the first deprotonation is the rate-determining step of DO3A1Pr, and this step was not facilitated a great deal by its new propionate arm.

pK_as Measured for DOTA and the DOTA Analogues. The modification of the pendant arms of DOTA to create DO4Pr significantly alters the structure and characteristics of the chelator. For example, the NMR pH titration on DO4Pr shows an increase of ca. 1 pK_a unit for titration of the second amine nitrogen proton relative to DOTA. The increase in the pK_a of the second macrocycle amine is important because the removal of these protons by reaction with base or via pendant arm mediated proton transfer has been proposed to be rate limiting for the metal loading reaction.[29] The increase in the pK_a value for the titration of the second amine proton of DO4Pr indicates that this proton is less reactive with base in the deprotonation reaction.

The titration of the G and F carboxylates is consistent with two amine protons on opposite sides of the macrocycle ring. In DO4Pr, the pK_as of the pendant arm carboxylates are increased relative to DOTA because of the increased distance from the positive charge on the protonated amines. Concomitantly, the F carboxylate pK_as of DO4Pr are essentially unchanged from the DOTA values because the F amines are not protonated.

The NMR pH titration also reveals that DOTA, the DOTA analogue 1,4,7-tris(carboxymethyl)-10-(butylaminocarboxymethyl)-1,4,7,10-tetraazacyclododecane (BD), and DO3A1Pr form **type II** complexes with potassium at basic pH while DO4Pr does not. In the first three compounds, an abrupt broadening and shifting of the chelate signals occurs at pHs where the last macrocycle amine proton is titrated (ca. pH 11). These changes are attributed to K^+ complexation by the fully deprotonated form of DOTA[13] and the DOTA analogues.[23] In contrast, DO4Pr signals become sharper and continue to shift at basic pHs, suggesting that this chelator does not complex K^+ in the same manner as DOTA. We propose that DO4Pr forms stable **type I** complexes of potassium.

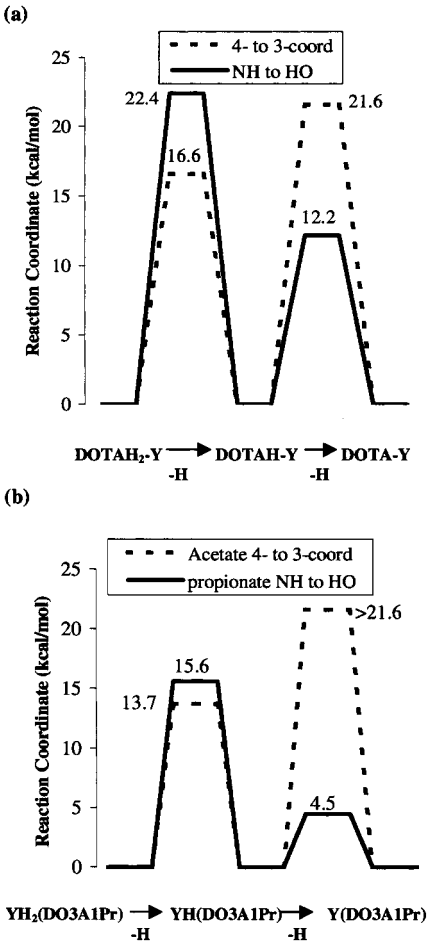

Figure 8. Schematic representation of the energetics of removal of the two macrocycle amine protons from (a) $YH_2(DOTA)^+$ and (b) $YH_2(DO3A1Pr)^+$.

The addition of a single methylene group to DOTA alters the pK_as of DO3A1Pr (Supporting Information Tables 3 and 4). For example, the two macrocycle amine nitrogen pK_as are increased by ca. 0.2 pK_a units on addition of the methylene group. This increase may be sufficient to affect metal loading because these amine protons must be removed to form the final **type II** complex.[23,29] Other acid dissociation constants are changed as well; the E and G carboxylate pK_as of DO3A1Pr are increased by 1 pK_a unit and the F carboxylate pK_as are decreased by 0.2 pK_a units compared to the DOTA values.

DO3A1Pr has pH-dependent structure alterations similar to those observed for BD.[23] Specifically, the titration of the E carboxylate of DO3A1Pr is accompanied by a deshielding chemical shift change in the F methylene proton signal (Supporting Information Table 4). Similar to BD, the deshielding chemical shift changes are attributed to the formation of a hydrogen bond with a macrocycle amine proton by the E carboxylate group.[23]

Yttrium Metal-Loading in DO4Pr and DO3A1Pr. The new calculations described above better reflect the improvement in the yttrium metal loading rate observed in DO3A1Pr and are summarized in Figure 8. Further refinement in rate predictions by ab initio methods may result from a more accurate estimation of the zero point energy and calculations of the macrocycle amine pK_as. The calculation of the pK_as of DOTA analogues is not a trivial matter because the molecule has six titratable

protons in close proximity. Recent work has shown that first principles density functional theory with the Poisson−Boltzmann continuum solvation model can be used to calculate the pK_as of a series of substituted uracil analogues (Jang et al., *J. Phys. Chem.*, in press). Similar calculations should be applicable to the DOTA analogues.

For DO4Pr, the ab initio calculations predicted a marked improvement in the rate of yttrium metal loading based on the improvement of the energetics of the proton-transfer with the propionate arms (3.9 kcal) compared to the acetate arms in DOTA (8.4 kcals).[32] The NMR results show that for DO4Pr, the G amine pK_a values are 9.6 and 11.9 compared to 9.7 and 10.9 in DOTA; the singly protonated form of DO4Pr is more stable by 1 pK_a unit than the singly protonated form of DOTA. Thus, the higher amine pK_a contributes to the stable **type I** complex formed by Y−DO4Pr.

For DO3A1Pr, the E and G amine proton pK_as were 9.9 and 11.1 compared to 9.7 and 10.9 for DOTA.[23] Therefore, at a given pH, the concentration of the doubly and singly protonated form of DO3A1Pr are higher than those of DOTA. At the same time the single propionate pendant group is a more facile proton-transfer mediator than the acetate arms and lowers the energy barriers for the deprotonation reactions. These two opposing factors may combine to yield the observed rate enhancement of 2-fold. By contrast, in the DOTA analogue BD, the amine pK_as are lower but the butylaminocarboxymethyl pendant arm is a poor proton-transfer mediator (the proton-transfer ability correlates with the ability of the pendant arm to form hydrogen bonds with the macrocycle amines). In this case the E and G amine BD pK_as are 9.0 and 10.7 versus to 9.7 and 10.9 for DOTA.[23] In our current model, a chelator that combines lower amine pK_as and good proton-transfer mediating properties in the pendant arms attached to the protonated macrocycle amines would yield the best improvement in the rate of metal loading and maintain high kinetic stability under physiological conditions.

Summary

This work focuses on developing an accurate predictive model for modification of DOTA pendant arms to improve the metal loading rates while maintaining the solution stability with a rigid tetraazamacrocycle scaffold. The results from the current work demonstrate that a relatively minor modification of DOTA improves the metal loading rate of the compound 2-fold. Further refinement of the calculations based on the results of this study will hopefully lead to development of improved chelators for radioimmunotherapy applications. Important to the rapid assessment of the multiple pendant arm modifications possible is the ability of the calculations to screen the best candidates for synthesis and NMR analysis.

Supporting Information Available: Listings of the geometry change from reactant to transition state in the proton transfer reaction of YH_2(DOTA) (Table 1), detailed energetics involved in deprotonation of YH_2(DOTA) (Table 2), acid dissociation constants and titration shifts for DO4Pr and DO3A1Pr (Tables 3 and 4), an illustration of the deprotionation pathway of YH_2(DO3A1Pr) (Figure 1), proton NMR spectra of DO3A1Pr as a function of pH (Figure 2), and an illustration of the deprotionation of pathways of YH(DOTA) (Figure 3). This material is available free of charge via the Internet at http://pubs.acs.org.

IC0010297